Identification of nonlinear phenomena in a stochastically excited beam system with impact

A. de Kraker*, N. van de Wouw, H.L.A. van den Bosch, D.H. van Campen
Department of Mechanical Engineering, Eindhoven University of Technology,
5600 MB Eindhoven, The Netherlands,
Email: kraker@wfw.wtb.tue.nl

Abstract

The response of strongly nonlinear dynamic systems to stochastic excitation exhibits many interesting characteristics. In this paper, an impacting beam system under broad and small banded, Gaussian noise excitation is investigated numerically as well as experimentally. The emphasis lies on frequency domain characteristics. Phenomena like multiple resonance frequencies and stochastic equivalents of harmonic and subharmonic solutions are found. A better understanding of such stochastic response characteristics is obtained by a comparison with nonlinear periodic response features. It is shown that these stochastic response phenomena can provide valuable information on periodic response characteristics of the system.

1. Introduction

Nonlinear dynamic systems under random excitation are frequently met in practice. The excitation randomness can vary from road profiles in vehicle motion, environmental loads, such as earthquakes and high building wind excitation, wave motions at sea exciting offshore structures or ships, or electric or acoustic noise exciting mechanical structures.

In this paper, a base excited beam system with a strong nonlinearity (elastic stop) is investigated. These kind of systems with a local nonlinearity are very regular in practice for example in case of gear rattle, ships-fender collisions and snubbers in satellite solar-arrays. Although the nonlinearity is local, the dynamic behaviour of the entire system is strongly influenced by it. Nonlinear periodic response phenomena of these kind of systems have been studied extensively, see Fey et al. [1996], Van de Vorst [1996], and Van Campen et al. [1997].

When stochastic excitations are applied to such systems, many unexpected interesting response phenomena can be observed. These phenomena are of specific interest because they shed light on the common characteristics of periodic and stochastic dynamic behaviour. As a consequence, the system's behaviour can be understood more thoroughly. For almost discontinuous nonlinearities, like an elastic stop, and (in our case band limited) random excitation, numerical integration is the only effective approach.
First the system will be introduced. In section 3, a brief survey of simulated periodic response characteristics will be given. The simulation procedure and -results will be discussed in sections 4 and 5. In sections 6 and 7 the experimental set-up is described and the experimental results are discussed and compared with simulation results. Finally, in section 8, we present some conclusions.

*Address all correspondence to this author.

2. The nonlinear beam system

2.1 System description

The system consists of a linear elastic beam, clamped onto a rigid frame, and an elastic stop (two half spheres), see figure 1. The

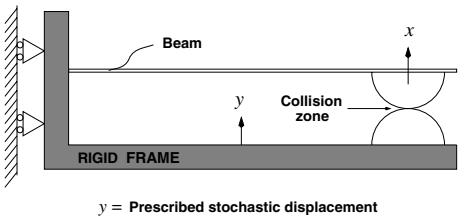

Figure 1: The nonlinear base excited beam system

system excitation comes from the prescribed stochastic displacement y of the rigid frame. The response x is the vertical displacement of the beam at the point of contact. In the next subsections 2.2, 2.3 and 2.4 the elastic beam model, a model for the elastic stop and finally the complete 1-dof model of the system will be presented.

2.2 The elastic beam

The elastic beam was modeled as a single-degree-of-freedom (SDOF) system using the Rayleigh-Ritz method. The system model can then be written as:

$$m\ddot{x} + b\dot{x} + kx = F \tag{1}$$

with mass $m = 37.75\ 10^{-3}\ [kg]$, stiffness $k = 736.3\ [N/m]$ and damping $b = 0.16\ [kg/s]$. The parameters m and k are tuned by means of experiments on the single beam system, and the damping parameter b was chosen according to the damping of the first and higher eigenmodes.

2.3 The elastic stop

The elastic stop is modeled using a Hertzian contact model [Hertz, 1895; Goldsmith, 1960]:

$$F = \frac{2}{3} E_r \sqrt{R_r}\, \delta^{1.5} = K_{\text{Hertz}} \delta^{1.5}, \qquad \delta \geq 0 \tag{2}$$

In equation (2), F is the contact force and $\delta = y - x, \delta \geq 0$ the relative displacement of the two colliding spheres, whereas the reduced Young's modulus E_r represents the material properties of both colliding bodies (made of PTFE). Furthermore, the reduced radius of curvature R_r represents the geometrical properties of the colliding bodies. The latter are defined as:

$$E_r = \frac{2}{\frac{1-\nu_1^2}{E_1} + \frac{1-\nu_2^2}{E_2}}\ ,\ R_r = \frac{R_1 R_2}{R_1 + R_2} \tag{3}$$

where R_i is the principal radius of curvature of body i, while E_i is the Young's modulus of body i and ν_i the Poisson's ratio of body i. The contact model (2) can be refined by adding a hysteretic damping term, see Lankarani and Nikravesh [1994], accounting for energy loss during collision, giving:

$$\begin{aligned} F &= K_{\text{Hertz}}\, \delta^{1.5} \left(1 + \frac{\mu}{K_{\text{Hertz}}} \dot{\delta}\right) \\ &= K_{\text{Hertz}}\, \delta^{1.5} \left[1 + \frac{3(1-e^2)}{4} \frac{\dot{\delta}}{\dot{\delta}^-}\right] \end{aligned} \tag{4}$$

in which e is the coefficient of restitution, a measure for energy dissipation. Moreover, $\dot{\delta}^-$ is the velocity difference of the two colliding bodies at the beginning of the impact. Both K_{Hertz} as well as e were estimated experimentally, using many collisions and least-squares estimation. In these measurements the indentation δ, the indentation velocity $\dot{\delta}$, and the contact force F were monitored, see figure 2. The parameter K_{Hertz} has been estimated by comparing F and δ at maximum indentation ($\dot{\delta} = 0$), assuming that the static contact force is proportional to $\delta^{1.5}$, see equation (2). The coefficient of restitution e has been estimated by considering the energy loss

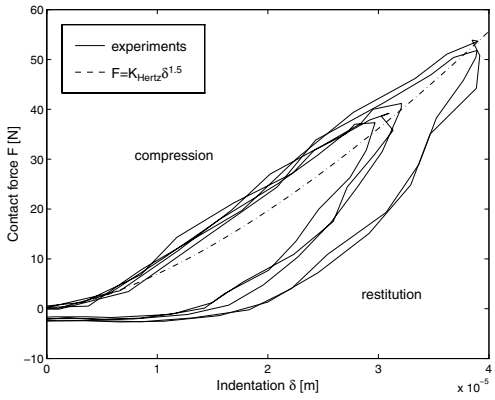

Figure 2: Measurement of several collisions to estimate K_{Hertz} and e

ΔT during collision (surface within the hysteresis loop):

$$\Delta T = \oint \mu\ \delta^{1.5}\ \dot{\delta}\ d\delta \tag{5}$$

Therefore, μ and e can be estimated from:

$$\mu = \frac{\Delta T}{\oint \delta^{1.5}\ \dot{\delta}\ d\delta};\ e = \sqrt{1 - \frac{\frac{4}{3}\ \mu \dot{\delta}^{-}}{K_{\text{Hertz}}}} \tag{6}$$

The actual estimated parameter values are: $K_{\text{Hertz}} \approx 2.1\ 10^8\ \text{N/m}^{1.5}$, $e \approx 0.5$.
The last value indicates that this damping is essential in the model.

2.4 The SDOF nonlinear dynamical model

The assembled nonlinear beam-impact model is visualized in figure 3 and its SDOF equation of motion becomes:

$$m\ddot{x} + b\dot{x} + kx + f(\delta) = b\dot{y} + ky \tag{7}$$
$$f(\delta) = \varepsilon(-\delta)\ F, \quad F \text{ from (4)}$$
$$\varepsilon(-\delta) = \begin{cases} 0 & \text{for} \quad \delta \leq 0 \\ 1 & \text{for} \quad \delta > 0 \end{cases}$$

It should be noted that K_{Hertz} considerably exceeds the linear beam stiffness k, indicating that the system is highly nonlinear.

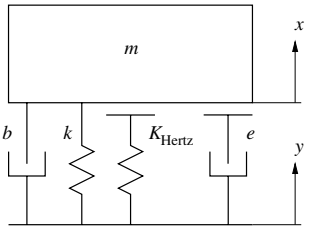

Figure 3: The SDOF model for the nonlinear beam system

3. Periodic response overview

To facilitate the interpretation of stochastic response phenomena, discussed later on in this paper, some periodic phenomena of the nonlinear beam system will be presented. Figure 4 shows the maximum absolute displacement x of periodic solutions as a function of excitation frequency for a 4-DOF model of a comparable nonlinear beam system, see Van de Vorst [1996]. Important response characteristics are the harmonic resonance peak, (1), and corresponding subharmonic resonances (1/2, 1/3) and superharmonic resonances (2), all with stable as well as unstable branches.

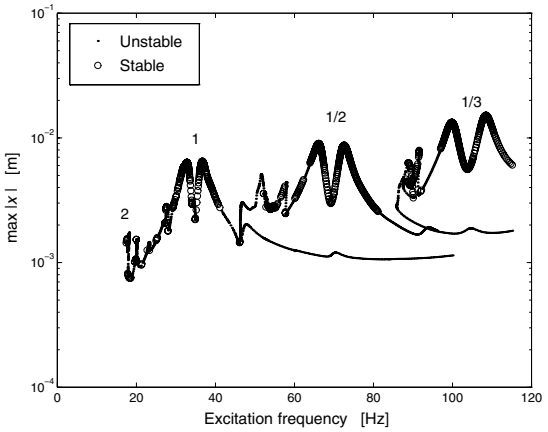

Figure 4: Maximum absolute displacements $|x|_{max}$ of periodic solutions of a 4-DOF model [Van de Vorst, 1996]

4. Simulation approach

4.1 Generation excitation signals

The base excitation of the system is assumed to be Gaussian, band-limited noise, as schematically shown in figure 5. For a de-

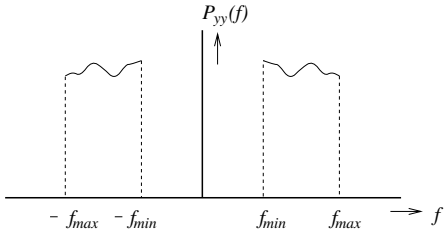

Figure 5: Excitation power spectral density $P_{yy}(f)$

sired excitation power spectral density function (p.s.d.) $P_{yy}(f)$ realizations can be generated using the method from Shinozuka [1972] and Yang [1972]. It implies that a one-dimensional Gaussian random process $y(t)$ with zero mean and one-sided p.s.d. : $G_{yy}(f)$ can be represented by a sum of cosine functions with a uniformly distributed random phase Φ. A realization $\bar{y}(t)$ of $y(t)$ can be simulated by:

$$\bar{y}(t) = \sqrt{\Delta f}\ \mathrm{Re}\{F(t)\} \tag{8}$$

in which $\mathrm{Re}\{F(t)\}$ is the real part of $F(t)$ and

$$F(t) = \sum_{k=1}^{N} \left\{ \sqrt{2G_{yy}(f_k)} e^{i\phi_k} \right\} e^{i2\pi f_k t} \tag{9}$$

is the finite complex Fourier transform of

$$\sqrt{2\ G_{yy}(f)}\ e^{i\phi} \tag{10}$$

where ϕ are the realized values of Φ.

4.2 Numerical time integration

A numerical time integration procedure is used to compute the response realizations $x(t)$ which are then used to calculate estimations for statistical moments, probability density function and power spectral density. Due to the random process stationarity and assumed ergodicity we can suffice with a single (long) realization and use time averaging.

For reasons of numerical efficiency, a constant step size, second-order Runge-Kutta scheme has been used for the integration. Due to the existence of a soft-spring-region (no contact) and a very stiff-spring-region (contact) we can distinguish two relevant stepsizes, which of course have been adjusted to match stability and accuracy conditions. Consequently, the time of impact has to be determined accurately to avoid crossing the contact border with the large time step. For this purpose the Hénon method is implemented within the integration routine.

This method is based on rearranging the differential equation without the nonlinearities (because a state just before impact will be observed) in such a way that the contact-distance $\delta = y - x$ becomes the **independent** variable whereas t becomes one of the **dependent** variables. From the last state before impact, the differential equation is integrated until $\delta = 0$ corresponding to t_{contact}, $\dot{x}(t_{\mathsf{contact}})$ and $x(t_{\mathsf{contact}}) = y(t_{\mathsf{contact}})$. Then a switch is made to the much smaller integration step-size, using these initial conditions.

5. Simulation results

A uniformly distributed $0 - 200$ Hz band excitation is applied to the system. For this system, this excitation can be seen as a broad band excitation. In figure 6, the p.s.d. of $y(t)$ is shown. An important property of the nonlinear response to Gaussian excitation is the fact that it will be non-Gaussian. Figure 7 illustrates the effect of the nonlinearity on the probability density function (PDF) of output δ. The non-Gaussian nature of the response also follows from higher-order moments like skewness and kurtosis. The estimates for the

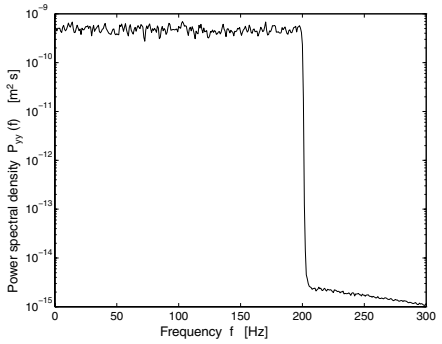

Figure 6: P.s.d. of 0-200 Hz band excitation $y(t)$

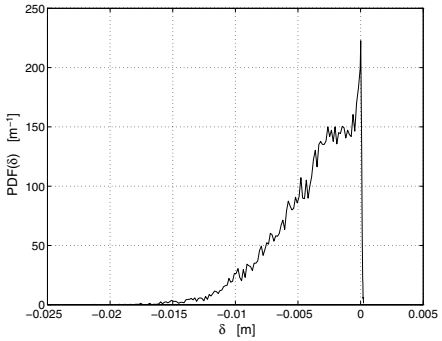

Figure 7: PDF of $\delta(t)$ for a 0-200 Hz band excitation

skewness and kurtosis are $\hat{\gamma}_\delta = -1.02$ and $\hat{\kappa}_\delta = 3.96$. They deviate considerably from the Gaussian values $\gamma = 0$ and $\kappa = 3$. A nonzero skewness points at an asymmetry of the PDF. This asymmetry of the response is a nonlinear characteristic of the system due to the elastic stop, see figure 8.

In literature very little attention is paid to frequency domain characteristics of nonlinear dynamic systems excited by stochastic processes. We will particularly focus on the observation and interpretation of these stochastic response phenomena, especially on one-sided power spectral densities (p.s.d.'s). The response p.s.d. of variable $\delta(t)$ is shown in figure 9, which admits two important observations:

1. The p.s.d. $P_{\delta\delta}(f)$ shows multiple resonance peaks.

2. It contains a considerable amount of low frequency energy (0-15 Hz) which is due to the asymmetry of the response process.

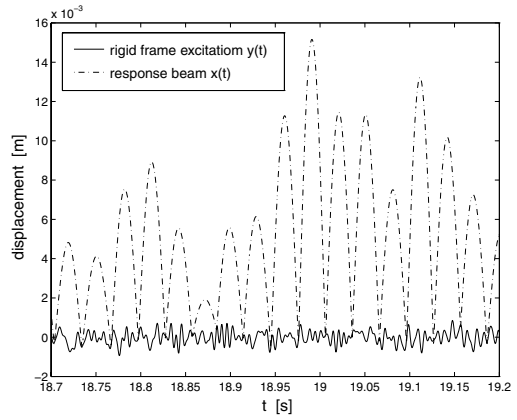

Figure 8: Parts of time series: 200 Hz band excitation $y(t)$ and response beam $x(t)$

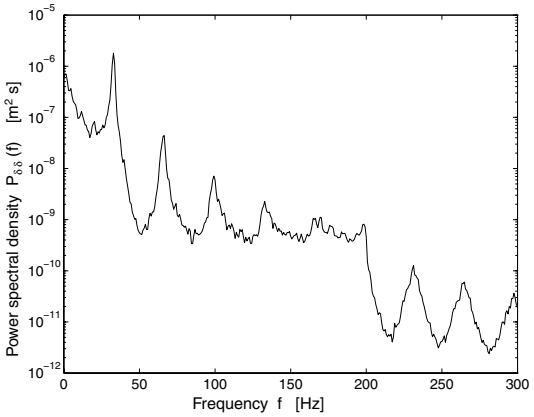

Figure 9: p.s.d. $\delta(t)$ for a 0-200 Hz band excitation

These are general stochastic response characteristics for weakly damped, strongly nonlinear systems with an asymmetric nonlinearity.

6. Experimental set-up

In the next section, simulation results will be validated by comparison to experimental results. Here the experimental set-up is presented schematically in figure 10. Again, a uniformly distributed Gaussian band limited excitation signal is generated numeri-

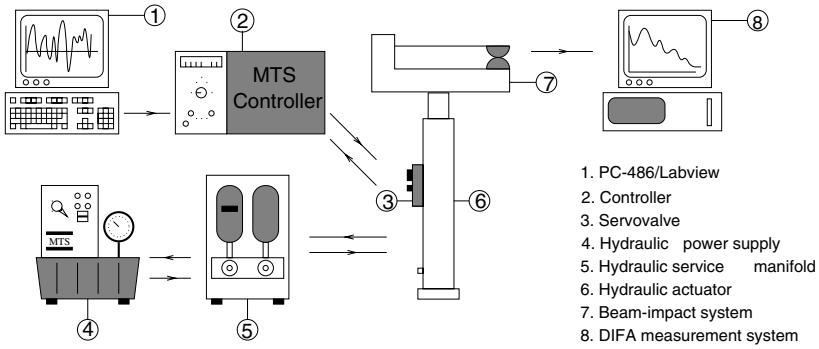

Figure 10: The experimental set-up

cally. This signal is sent to a controller which controls a servo valve using feedback information from an internal displacement transducer. The servo valve provides the input for the hydraulic actuator by controlling the oil flow of the hydraulic power supply. A hydraulic service manifold connects the hydraulic power supply and the servo valve. This service manifold reduces fluctuations and snapping in the hydraulic lines during dynamic programs. All measurements are monitored using a data acquisition software package [DIFA, 1992]. Figure 11 shows

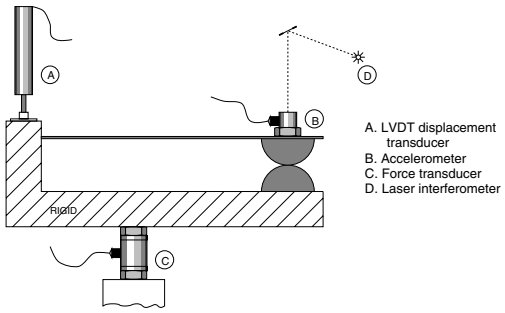

Figure 11: The measurement equipment

the measurement equipment mounted on the beam-impact system. A Linear Variable Differential Transformer (LVDT) measures the displacement of the rigid frame. The displacement and velocity of the beam, at the point of contact, are measured by a laser interferometer. Furthermore, the acceleration of the beam is measured by an accelerometer. A force transducer is used to measure the force acting on the rigid frame.

7. Experimental results

Again, a 200 Hz (broad) band excitation was applied. The realized base-excitation spectrum is given in figure 12. This is not a uniform spectrum anymore because hydraulic actuator behaves like a first-order low-pass filter. Therefore, it is necessary to repeat the simulations with these rigid frame excitation spectra for a correct comparison between simulations and experiments.

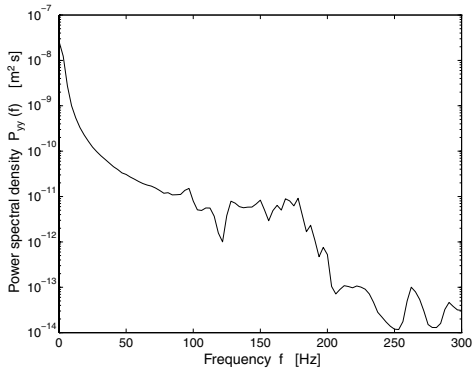

Figure 12: Power spectral density of the 200 Hz band excitation

The estimates of the probability density functions of both the excitation $y(t)$ and the response $\delta(t)$ are shown in the figures 13 and 14, respectively. Again the results clearly display the fact that the response is strongly non-Gaussian. Both the simulated and

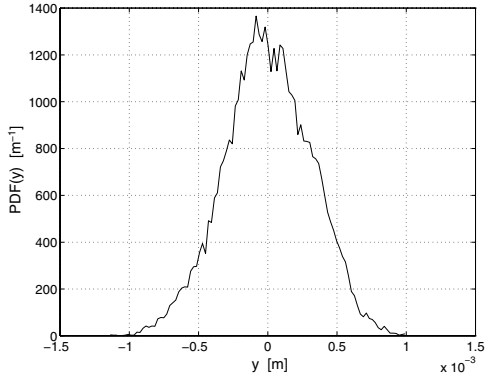

Figure 13: Probability density function of the measured 0-200 Hz band excitation $y(t)$

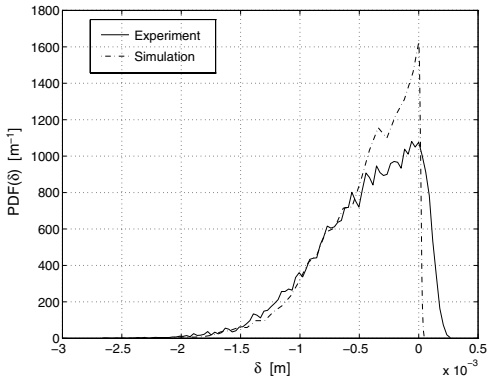

Figure 14: Probability density function of $\delta(t)$ for a 0-200 Hz band excitation

measured response p.s.d.'s are shown in figure 15. The most important response phenomena like multiple resonance peaks and the presence of a large amount of low frequency energy are clearly visible in both experimental and simulation results. However, the non-uniformity of $P_{yy}(f)$ obstructs the observation of the second characteristic. Figures 14 and 15 show that the experimental and numerical results correspond to a large extent. The experimental resonance peak around 120 Hz is due to the second harmonic resonance of the beam system, related to the second eigenfrequency[1]. Of course, this resonance peak is missing in the simulation results as a consequence of SDOF modeling.

[1]In case of a nonlinear system, one cannot speak of *eigenfrequencies*. However, here this terminology is used for a frequency at which the system resonates.

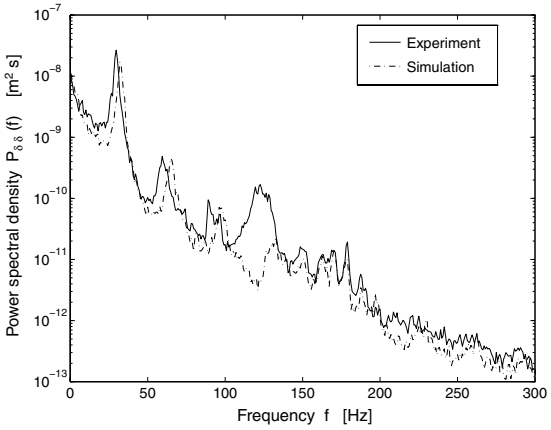

Figure 15: Power spectral density of the response $\delta(t)$ to the 200 Hz band excitation

Finally, also two specific narrow-band excitations were considered. Firstly, a band excitation $[23 \leq f \leq 43]$ [Hz], covering the major part of the harmonic resonance peak was applied. The relating response p.s.d. again exhibits multiple resonance peaks. Secondly, a band excitation $[56 \leq f \leq 76]$ [Hz], covering the major part of the $\frac{1}{2}$ subharmonic resonance peak was applied; the relating response p.s.d. is shown in Figure 16. This

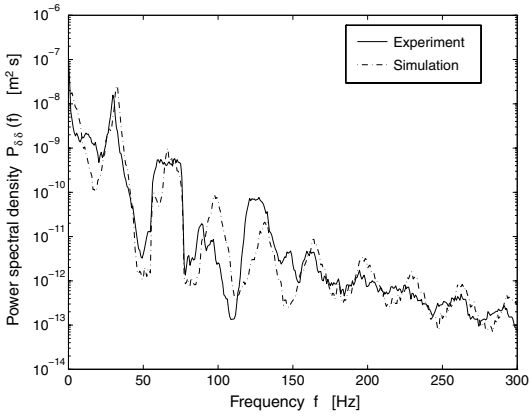

Figure 16: Power spectral density of the response $\delta(t)$ to the 56-76 Hz band excitation

figure clearly displays a 'stochastic $\frac{1}{2}$ subharmonic' phenomenon in the response (for both

simulation and experiment), which can be related to the $\frac{1}{2}$ subharmonic resonance peak in Figure 4. These response characteristics to narrow-banded excitation illuminate the origin of the multiple resonance peaks in the response to broad band excitations. For more information on this we refer to Van de Wouw et al. [1997].

8. Conclusions

We have applied Gaussian band limited excitations to a strongly nonlinear impacting system. The derived nonlinear model is SDOF. Many interesting, specifically nonlinear, stochastic response phenomena have been investigated both numerically as well as experimentally. Especially frequency domain characteristics have been emphasized.

Both broad- and narrow-band excitations are applied in order to discriminate the origin of certain frequency domain response characteristics. Nonlinear stochastic phenomena like multiple resonance peaks and a high-energy, low-frequency response content are found applying broad-band excitations.

Stochastic equivalents of harmonic and subharmonic solutions are found. With respect to all these response characteristics, the numerical and experimental results agree to large extent. The observed phenomena can also be found in systems with other one-sided nonlinearities, see Van de Wouw et al. [1997]. Therefore, these characteristics can give insight in the nonlinear stochastic behaviour of a large class of nonlinear dynamic systems.

Future research will involve the extension of the model to include higher modes of the beam. This extension will improve the response characteristics around the second harmonic resonance frequency. Moreover, such a multi-degree-of-freedom model might also describe the system better for lower frequencies, because these higher modes affect the behaviour in the lower frequency range for periodic excitations, see Figure 4.

References

DIFA (1992). *FA100 User Manual*. DIFA Measuring Systems, Breda, The Netherlands.

Fey, R., Van Campen, D., and De Kraker, A. (1996). Long term structural dynamics of mechanical systems with local nonlinearities. *Trans. ASME, J. Vibration and Acoustics*, **118(2)**, 147–153. Also publ. in: Proc. Winter Annual Meeting ASME, Anaheim (Calif., USA), 8-13 Nov., DE-Vol. 50, AMD-Vol. 44, eds. R.A. Ibrahim and N.S. Namachchivaya, 1992, pp. 159-167.

Goldsmith, W. (1960). *Impact: The Theory and Physical Behaviour of Colliding Solids*. E. Arnold Ltd., London.

Hertz, H. (1895). *Gesammelte Werke, vol. 1: Schriften Vermischten Inhalts*. J.A. Barth, Leipzig, Germany (German).

Lankarani, H. and Nikravesh, P. (1994). Continuous contact force models for impact analysis in multibody sytems. *Nonlinear Dynamics*, **5**, 193 – 207.

Shinozuka, M. (1972). Monte carlo solution of structural dynamics. *Computers & Structures*, **2**, 855–874.

Van Campen, D., De Kraker, A., Fey, R., Van de Vorst, E., and Van der Spek, J. (1997). Long-term dynamics of nonlinear mdof engineering systems. *Chaos, Solitons and Fractals; Special issue on Nonlinearities in Mechanical Engineering*, **8(4)**, 455–477.

Van de Vorst, E. (1996). *Long term dynamics and stabilization of nonlinear mechanical systems*. Ph.D. thesis, Eindhoven University of Technology, The Netherlands.

Van de Wouw, N., De Kraker, A., and Van Campen, D. (1997). Nonlinear phenomena in a stochastically excited dynamic system. In *Proc. 1997 ASME Int. Mechanical Engineering Congress and Exposition, Dallas (USA), DE-Vol. 95, AMD-Vol. 223, 16-21 Nov. 1997*, pp. 151–158. eds. W.C. Xie, N.S. Namachchivaya and O.M. O'Reilly.

Yang, J.-N. (1972). Simulation of random envelope processes. *Journal of Sound and Vibration*, **21(1)**, 73–85.